Geometrical determinant of nonlinear synaptic integration in human cortical pyramidal neurons

Jaeyoung Yoon[1,2,*], et al.[†]

[1] McGovern Institute for Brain Research, Massachusetts Institute of Technology, Cambridge, MA 02139, USA.
[2] Present address: F. M. Kirby Neurobiology Center, Boston Children's Hospital, Harvard Medical School, Boston, MA 02115, USA.
[*] Correspondence: jy.yoon@tch.harvard.edu
[†] *Full author list to be determined*

Abstract

Neurons integrate synaptic inputs and convert them to action potential output at electrically distant locations. The computational power of a neuron is hence enhanced by subcellular compartmentalization and nonlinear synaptic integration, but the biophysical determinants of these features in human neurons are not completely understood. By examining the synaptic input-output function of human neocortical pyramidal neurons, we found that the nonlinearity threshold at the soma was linearly determined by the shortest path distance from the synapse to the apical trunk, and the slope of this relationship was consistent throughout the dendritic arbor. Analogous rules were found from both supragranular and infragranular layers of the rodent cortex, suggesting that these represent a fundamental property of pyramidal neurons. Additionally, we found that neurons associated with tumor or epilepsy had distinct membrane properties, but the nonlinearity threshold was shifted in amplitude such that the slope of its relationship with synaptic distance remained consistent.

Fig. 1
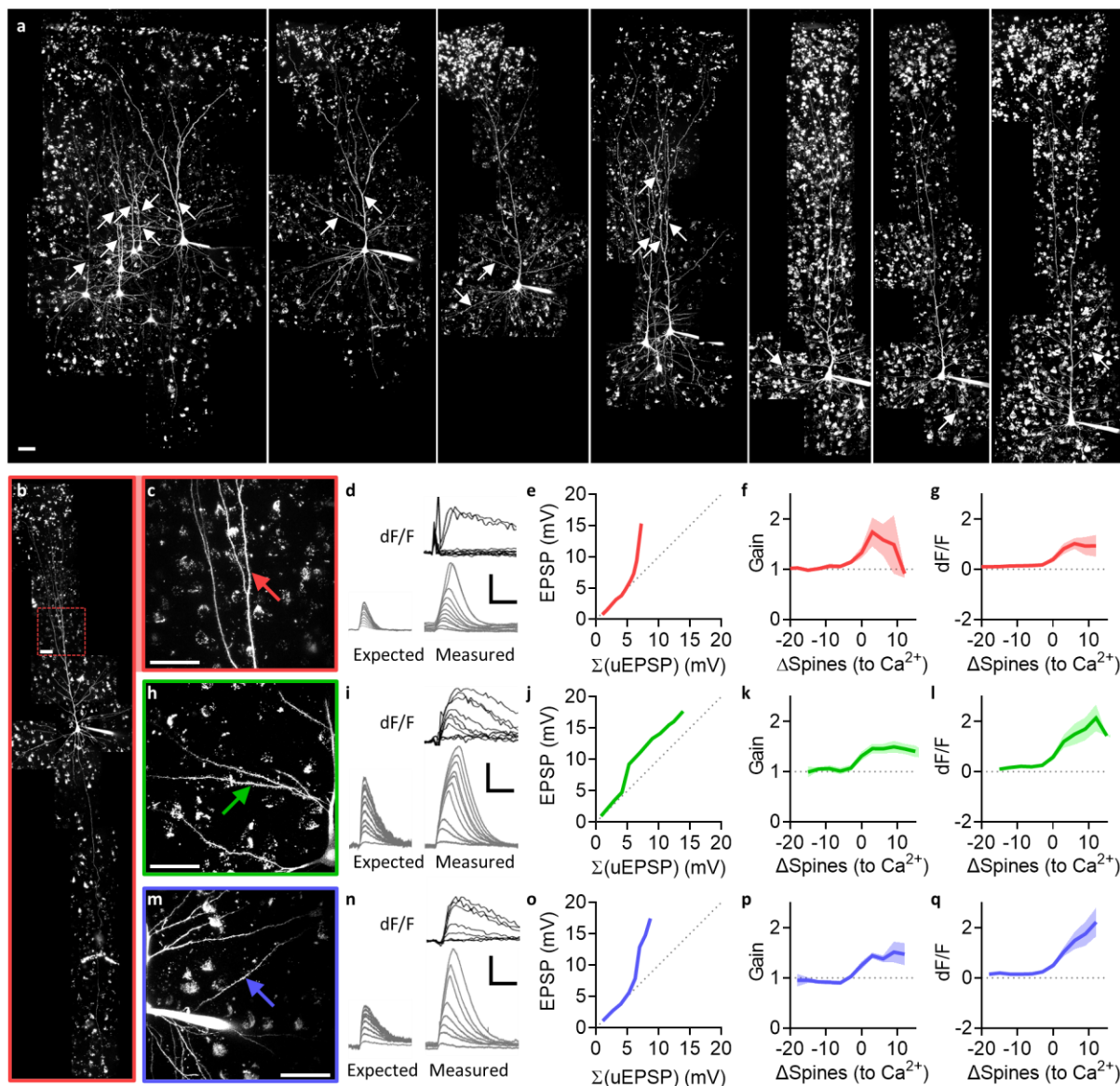
27 **Figure 1.** Synaptic integration at human neocortical layer 2/3 pyramidal neurons (L2/3 PN). **(a)**
28 Representative examples of human L2/3 PNs. Scale bar, 50 µm. Scale bar definitions are
29 consistent throughout all images in all figures. Arrows indicate the center of synaptic spines
30 that were activated by 2-photon glutamate uncaging (2PGU), which typically spanned
31 approximately 30-50 µm along the length of the branch. The high background fluorescence in
32 the human cortex is caused by lipofuscin aggregates on the neuronal somata; see **Fig. 4** for
33 comparison with the rodent cortex. **(b-c)** Representative example of 2PGU at the apical tuft.
34 **(d)** Representative data from the dendrite in panel **c**, with the expected EPSP (left) calculated
35 from the arithmetic sum of unitary EPSPs (uEPSP) recorded from each respective spine, and
36 the measured EPSP (right, bottom) recorded by simultaneous activation of multiple spines,
37 along with the associated fractional change in fluorescence (dF/F) from intracellular calcium
38 imaging at the parent dendrite (right, top). Scale bars, 50 ms, 5 mV, 1.0 dF/F. **(e)** Representative
39 data from the same dendrite as in panels **b-d**, with the measured EPSP plotted against the
40 expected EPSP from the arithmetic sum of uEPSPs. **(f)** Grouped average of synaptic gain from
41 all apical tuft dendrites (n = 24). Gain was defined as the ratio of measured vs. expected EPSP.
42 The number of activated spines were aligned to the nonlinearity threshold at which Ca^{2+} signal
43 was first observed at the synaptic site. **(g)** Grouped average of dF/F, associated with data
44 shown in panel **f**. **(h-l)** Similar to panels **c-g**, but from oblique dendrites (n = 16) branching
45 from the apical trunk. **(m-q)** Similar to panels **c-g** or **h-l**, but from basal dendrites (n = 20)
46 extending from the soma.

47

Fig. 2
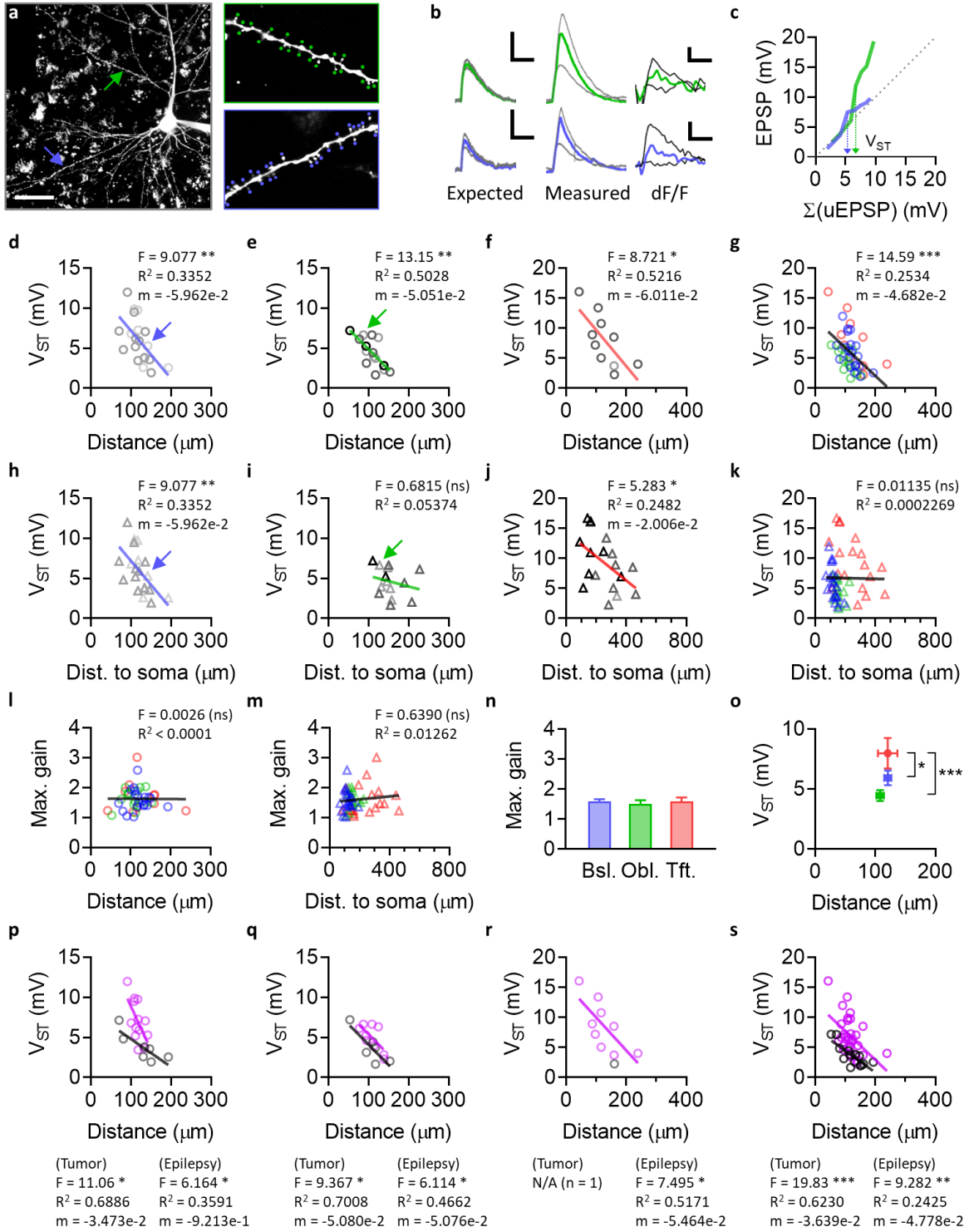
Figure 2. Somatic depolarization at supralinearity threshold (V_{ST}) is linearly determined by synaptic distance from the apical trunk. **(a)** Representative example of a human L2/3 PN. Two different uncaging locations, one at a basal dendrite (blue) and another at an oblique dendrite (green), are indicated by arrows. Scale bar, 50 μm (left). Dots indicate uncaging spots (right). **(b)** Representative traces of expected and measured EPSP, along with associated dF/F, from the branches shown in panel **a**. Scale bars, 50 ms, 5 mV, 0.1 (top) or 0.5 (bottom) dF/F. **(c)** Measured EPSP vs. expected EPSP from the sum of uEPSPs, from the same branches as in panels **a-b**. V_{ST} was defined as the expected EPSP at synaptic nonlinearity threshold indicated by the local Ca^{2+} signal. The expected EPSP from the sum of uEPSPs was used for the definition of V_{ST} to determine the correct threshold irrespective of the nonlinear gain. **(d-g)** V_{ST} plotted against synaptic distance. Synaptic distance was defined as the shortest projected path distance along the dendrite from the synapse to the apical trunk. Notably, the linear regressions in panels **d-f** had similar slopes in all groups (F = 0.06380, P = 0.9383), and consequently also in panel **g**. **(d)** V_{ST} vs. synaptic distance at basal dendrites. Shades of symbols indicate branch order (darker to lighter, 1st to 4th; throughout panels **d-f** and **h-j**), which was not correlated with V_{ST} in any group. **(e)** V_{ST} vs. synaptic distance at oblique dendrites. **(f)** V_{ST} vs. synaptic distance at apical tuft dendrites. **(g)** Data shown in panels **d-f**, taken together for comparison. **(h-k)** similar to panels **d-g**, but plotted instead against the distance from synapse to soma instead of the apical trunk; panel **h** was reproduced from panel **d** as the path distance to the soma or the apical trunk are approximately identical for basal dendrites, as the position of the soma was defined as the center of mass of its boundary. In panel **j**, synapses located at the nexus are also included, which were excluded from panel **f** due to having zero synaptic distance per definition. **(l)** Maximum gain vs. synaptic distance to the apical trunk. **(m)** Maximum gain vs. distance to soma. **(n)** Maximum gain at basal, oblique, and tuft dendrites. **(o)** Average V_{ST} at basal, oblique, and tuft dendrites. **(p-s)** Same data as in panels **d-g**, but grouped according to tissue origin in terms of tumor (black) or epilepsy (purple). Neurons from the nonpathological part of the neocortex associated with epilepsy had a tendency of higher V_{ST} for a given synaptic distance, compared to those from tumor tissue.

Fig. 3
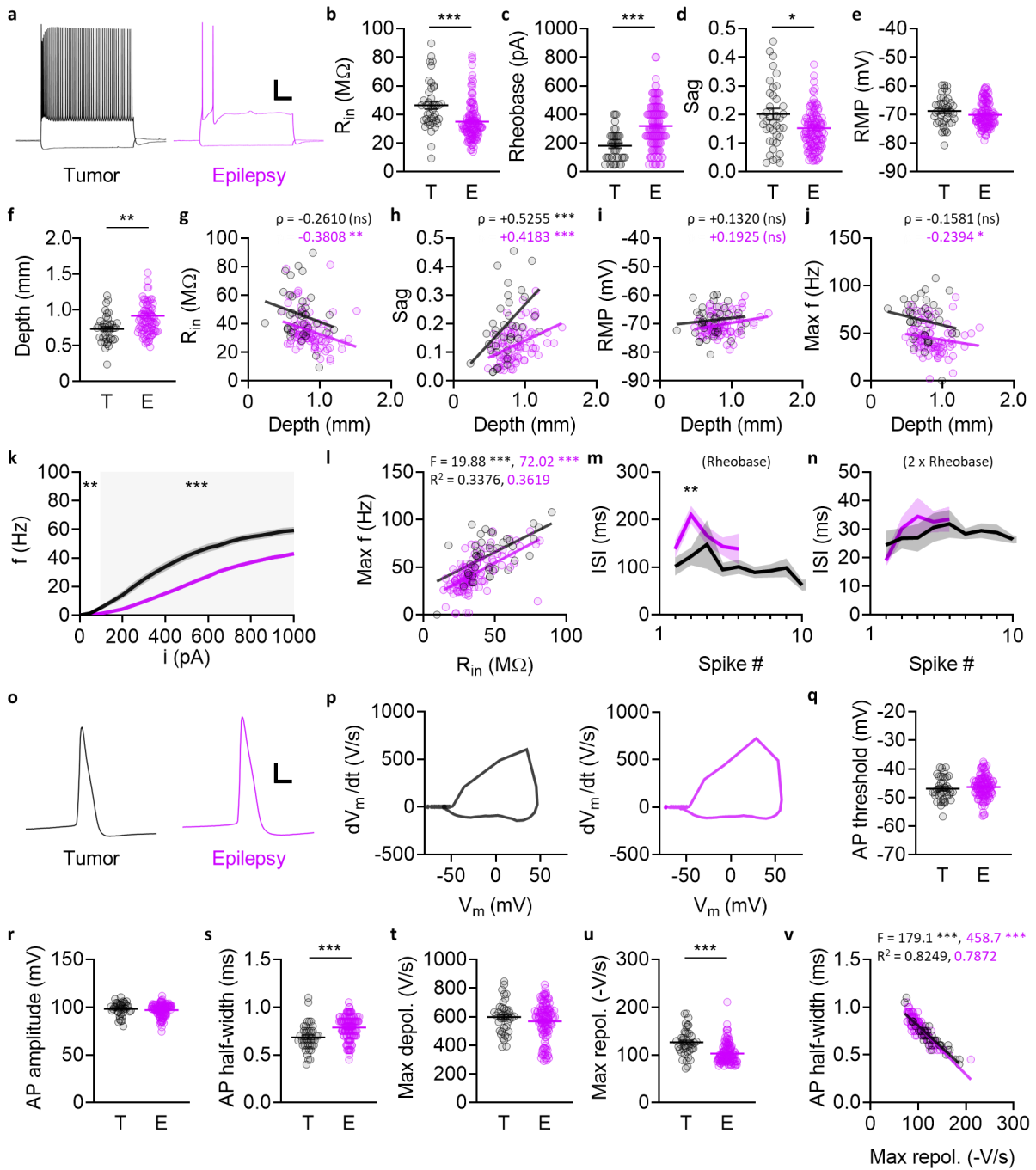
Figure 3. Intrinsic membrane properties of human L2/3 PN, from tumor (black) or epilepsy (purple). For more detailed patient and tissue information, see **Table 1**. Note that tissue from both tumor and epilepsy patients originated from parts of the neocortex that were clinically categorized as nonpathological. **(a)** Representative traces of membrane potential responses to somatic step current injection (-250 pA, +1000 pA). Scale bar, 20 mV, 200 ms. The example to the right was taken from the same cell as in **Fig. 1b**. **(b)** Input resistance (R_{in}). See Methods for R_{in} calculation. **(c)** Rheobase, with current step resolution of 50 pA. **(d)** Sag ratio. See Methods for the definition of sag ratio. **(e)** Resting membrane potential (RMP). **(f)** Cortical depths of recorded L2/3 PNs included in the current study. Cortical depth of a cell was defined as the linear distance between the pial surface and the soma, extrapolated from the line between the soma and the nexus. The depth of one outlier in the tumor group (235 μm) and its identity as an L2/3 PN was verified with the whole-cell 2-photon image of the cell, accompanied by other L2/3 PNs deeper in the vicinity, all of which had dendritic arbors that were intact up to the pia mater and in plane. **(g-j)** Intrinsic membrane properties, plotted against cortical depth. Linear regressions are presented for visual aid, but correlations were assessed using Spearman's rank correlation coefficient. **(g)** R_{in}. **(h)** Sag ratio. **(i)** RMP. **(j)** Peak firing rate. **(k)** Firing rate in response to somatic current injection. L2/3 PN firing rates were significantly lower in epilepsy compared to tumor ($P < 0.001$ each for all i ≥ 100 (pA), $P < 0.01$ for i = 50). **(l)** Peak firing rate, plotted against R_{in}. **(m)** Inter-spike interval (ISI) at rheobase. **(n)** ISI at 2*rheobase. **(o)** Representative traces of single action potentials (AP) from human L2/3 PNs. For each cell, the first AP generated at rheobase was taken for analysis. Scale bar, 20 mV, 1 ms. The example to the right was taken from the same cell as in **Fig. 2a**. **(p)** Representative examples of AP waveforms calculated from the same traces shown in panel **o**, presented as the derivative of the membrane potential with respect to time (dV_m/dt) plotted against the membrane potential (V_m). **(q)** AP threshold. AP threshold was defined as the V_m at which dV_m/dt reached 10 (V/s). **(r)** AP amplitude (from AP threshold to AP peak). **(s)** AP half-width. **(t)** Maximum rate of depolarization. **(u)** Maximum rate of repolarization. **(v)** AP half-width plotted against the maximum rate of repolarization.

Fig. 4
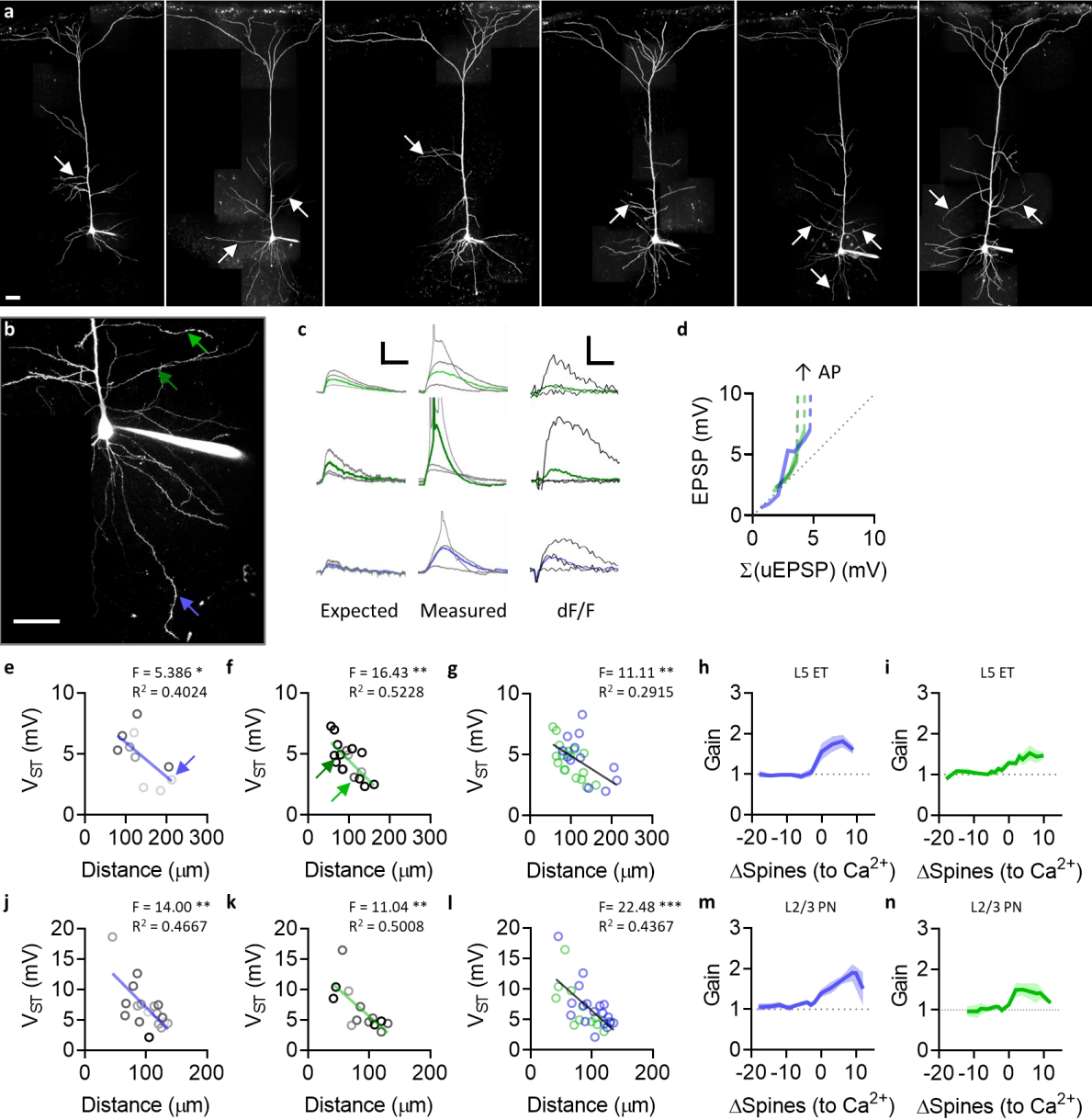
112   **Figure 4.** Somatic depolarization at supralinearity threshold (V_{ST}) is determined by synaptic
113   distance from the apical trunk, analogously for supragranular and infragranular PNs in the
114   rodent cortex in addition to human PNs. **(a)** Representative examples of L5 extratelencephalic
115   (ET) PNs, from the rat temporal association area (TeA). Arrows indicate uncaging locations.
116   Scale bar, 50 μm. Compare with **Fig. 1** for the difference in background fluorescence caused
117   by lipofuscin in the human cortex. **(b)** Representative example of a rat L5 ET PN, with three
118   different uncaging locations; one on a basal dendrite, and two on separate oblique dendrites.
119   **(c)** Representative traces from synaptic activation in dendrites shown in panel **a**. Scale bars,
120   50 ms, 5 mV, 0.5 dF/F. **(d)** Measured EPSP vs. expected EPSP from the sum of uEPSPs, from the
121   same dendrites as in panels **b-c**. **(e-g)** V_{ST} vs. synaptic distance as defined in **Fig. 2**, in rat L5 ET.
122   The slopes of the regressions in panels **e** and **f** were not different (F = 0.5381, P = 0.4700). **(e)**
123   Basal dendrites. **(f)** Oblique dendrites. **(g)** Data shown in panels **e-f**, overlaid for comparison.
124   **(h)** Synaptic gain, at basal dendrites shown in panel **e**. **(i)** Synaptic gain, at oblique dendrites
125   shown in panel **f**. **(j-n)** Similar to panels **e-i**, but from rat L2/3 PNs instead of L5 ET. The slopes
126   of the regressions in panels **j** and **k** were not different (F = 0.1038, P = 0.7498). **(j)** Basal
127   dendrites. **(k)** Oblique dendrites. **(l)** Data shown in panels **j-k**, overlaid for comparison. **(m)**
128   Synaptic gain, at basal dendrites shown in panel **j**. **(n)** Synaptic gain, at oblique dendrites
129   shown in panel **k**.

130

131   **Table 1**

ID	Age	Sex	Area	Hemi.	Medications (AED)	Diagnosis	n (cells/humans)
						(Tumor)	43/5
						(Epilepsy)	119/17
						(Total)	162/22

132   **Table 1.** Patient and tissue information. (redacted from this preview)

133